Biosensors and Bioelectronics 155 (2020) 112094

Contents lists available at ScienceDirect

Biosensors and Bioelectronics

journal homepage: http://www.elsevier.com/locate/bios

Nano-biosensor for the *in vitro* lactate detection using bi-functionalized conducting polymer/N, S-doped carbon; the effect of αCHC inhibitor on lactate level in cancer cell lines

Khalil K. Hussain [a,1], N.G. Gurudatt [a], Mahmood H. Akhtar [a], Kyeong-Deok Seo [a], Deog-Su Park [b], Yoon-Bo Shim [a,b,*]

[a] Department of Chemistry, Pusan National University, Busan, 46241, South Korea
[b] Institute of BioPhysio Sensor Technology, Pusan National University, Busan, 46241, South Korea

ARTICLE INFO

Keywords:
Lactate sensor
LDH immobilization
α-Cyano-4-hydroxycinnamate (αCHC)
N
S -doped porous carbon
Bifunctional conducting polymer

ABSTRACT

A robust amperometric sensor was developed for the lactate detection in the extracellular matrix of cancer cells. The sensor was fabricated by separately immobilizing nicotinamide adenine dinucleotide (NAD^+) onto a carboxylic acid group and lactate dehydrogenase (LDH) onto an amine group of bi-functionalized conducting polymer (poly 3-(((2,2':5′,2″-terthiophen)-3′-yl)-5-aminobenzoic acid (pTTABA)) composited with N, S-doped porous carbon. Morphological features of the composite layer and sensor performance were investigated using FE-SEM, XPS, and electrochemical methods. The experimental parameters were optimized to get the best results. The calibration plot showed a linear dynamic range between 0.5 μM and 4.0 mM with the detection limit of 112 ± 0.02 nM. The proposed sensor was applied to detect lactate in a non-cancerous (Vero) and two cancer (MCF-7 and HeLa) cell lines. Among these cell lines, MCF-7 was mostly affected by the administration of lactate transport inhibitor, α-cyano-4-hydroxycinnamate (αCHC), followed by HeLa and Vero, respectively. Furthermore, the effect of αCHC concentration and treatment time on the lactate level in the cell lines were demonstrated. Finally, cytotoxicity studies were also performed to evaluate the effect of αCHC on cell viability.

1. Introduction

Cancer microenvironment is complex, composing of different types of cells and molecules, which facilitates cancer cells to reprogram the blood vessels and assist tumor growth (Whiteside et al., 2008). Of the various soluble molecules located in the tumor microenvironment, lactate is of importance due to its vital role in cancer progression. The high utilization of extracellular glucose by cancer cells results in the accumulation of extracellular lactate, therefore, altering the pH of cancer microenvironment to 6.0–6.5 (Romero et al., 2016). The acidic microenvironment facilitates signals for angiogenesis, act as a metabolic fuel, loss of the T-cell function, and induces immunosuppression (Estrella et al., 2013; Hirschhaeuser et al., 2011). However, under normal conditions, lactate is cleared mainly by the liver at a rate of 320 mmol/L/h and to a lesser extent by the kidneys (Van hall et al., 2010). Furthermore, lactate is transported across the cell plasma membrane in the human body by the action of monocarboxylate transporters (MCTs). Various cancer cells display different types of MCTs. Among them, MCT1 and MCT4 are the widest MCT isoforms expressed in cancer cells (Pérez et al., 2016). Recently, MCT inhibitors were considered as an emerging route in cancer therapy by blocking lactate transport across the cell membrane, therefore, inducing apoptosis in tumor cells due to the intracellular acidosis. To date, several MCT inhibitor drugs have been reported, including AR-C155858, AR-C117977, AZD3965 (AstraZeneca), and a-cyano-4-hydroxycinnamic acid (αCHC) (Galluzzi et al., 2013). Of them, αCHC is cheap, selective, and showed an excellent anti-tumor activity in various cancers, such as glioblastoma (Colen et al., 2011), breast cancer (Hamdan et al., 2013), and prostate tumor (Kim et al., 2012), however, the drug is not approved for clinical trial, possibly due to the insufficient clinical evidences. Therefore, there is great need to develop a highly sensitive and selective method for lactate detection especially in biomedical applications, such as evaluating the cytotoxic effect of αCHC on cancer cells.

Analytical methods commonly employed for the lactate detection

* Corresponding author. Department of Chemistry and Institute of Bio Physio Sensor Technology (IBST), Pusan National University, Busan, 46241, South Korea.
E-mail address: ybshim@pusan.ac.kr (Y.-B. Shim).
[1] Present address: Department of Biosciences, MRC Centre for Medical Mycology, University of Exeter, Exeter, EX4 4QD, UK.

https://doi.org/10.1016/j.bios.2020.112094
Received 10 January 2020; Received in revised form 11 February 2020; Accepted 12 February 2020
Available online 16 February 2020
0956-5663/© 2020 Elsevier B.V. All rights reserved.

include high performance liquid chromatography (Milagres et al., 2012), electric biosensor (Braendlein et al., 2017), and chemiluminescence (Wu et al., 2005). Although these methods provide good results, but they are time consuming, costly, required sample pretreatment, and trained personals. Alternatively, electrochemical biosensors are considered as simple, direct, selective, real time detection method, and have the ability of miniaturization for on-site medical diagnosis. Due to these advantages, various enzyme-based biosensors have been reported for the lactate detection (Niklaus et al., 2008; Rathee et al., 2016). However, most of them suffer from a short dynamic range and high detection limit. One of the possible reasons is that the amount of enzyme and cofactor on the electrode active surface area is very less or inadequate, which reduces the performance of the sensor probe. To overcome such shortcoming, it is crucial to develop an alternative improved biosensor with catalytic electrode materials, which possess a wider dynamic range, the lower detection limit, and adequate amount of immobilized enzyme onto the electrode active surface. In addition, other electrochemical methods to overcome these shortages were also reported using a label free detection for various biomarker protein (Zhang et al., 2019), cancer cell capture (Sun et al., 2019), etc.

To date, conducting polymers (CPs) have been received much attention in the development of electrochemical biosensor due to their unique electrical properties, inexpensive, and excellent matrices for stable biomolecule immobilization without loss of their biological functions. These beneficial properties enabled them to find a wide range of applications. Of these CPs, polyterthiophene (Kwon et al., 2006; Moon et al., 2018) is non-toxic, robust, and highly stable compared to that of polyaniline (Shim et al., 1990) and poly pyrrole (Park et al., 1993). Usually, the polyterthiophene backbone was functionalized with a single group of - COOH or $–NH_2$ (Akhtar et al., 2016; Naveen et al., 2017a, b), which were used to immobilize biomolecules, such as enzyme or host proteins. However, it mostly immobilizes a single modifier limitedly, since they have a single binding site. Otherwise, when someone needs the binding of two or three different biomolecules on a polymer layer, it demands to share a binding site by different biomolecules, such as cofactor/enzyme. In this case, the analytical performance is lessened due to the smaller or inadequate immobilized number of biomolecules. Hence, to improve the performance of multi-functional sensor probe, a bi-functionalized CP bearing different functional groups in a single monomer molecule is efficient for the distinct immobilization of cofactor and enzyme together onto each functional group. It eventually can enhance the overall sensor performance by increasing immobilized amounts on the sensor probe. Thus, we firstly synthesize the bi-functionalized CP and develop a new lactate biosensor.

Although functional CPs are excellent as biosensor electrode material, they have mostly lower conductivity than that of metal or carbon electrode materials. Thus, it is one of ways to enhance the conductivity and the catalytic property to prepare the composite electrode using CPs and catalytic carbon. The porous carbon is attractive due to their cost effective, large surface area, and stability, however, they sometimes exhibited low electrocatalytic activity. To overcome such disadvantage, a new type of porous carbon material has been synthesized doped with heteroatoms (N, B, or S) to promote the catalytic and electric property of the carbon materials (Naveen et al., 2017a, b). Usually, N and S atoms possess extra valence electrons and more electronegativity relative to that of mere porous carbon, hence they can effectively modulate the charge distribution of sp^2 carbon framework, induce the structural variation, increase electron transfer rate, and enhance conductivity, resulting in a highly active electrocatalytic property toward various molecules including biologicals.

In the present study, an amperometric lactate sensor was fabricated by separately bonded nicotinamide adenine dinucleotide (NAD^+) and lactate dehydrogenase (LDH) onto (COOH) and (NH_2) terminals of the bi-functionalized CP (poly 3-((2,2′:5′,2″-terthiophen)-3′-yl)-5-aminobenzoic acid (pTTABA)) coated on the N, S-doped porous carbon layer for the first time. The signal was monitored for the electrochemical oxidation of NADH generated by the enzymatic reaction at the electrode surface. The performance of the proposed sensor was compared between hetero atoms-doped porous carbon (DPC) and mere porous carbon powders as well as between single and bi-terminal immobilization on pTTABA. The proposed sensor was evaluated to determine the lactate concentration in normal (Vero) and cancer (MCF-7 and HeLa) cells. Finally, the effect of αCHC on the lactate transport was investigated employing same cell lines, and time dependency and concentration profile were obtained for αCHC.

2. Experimental

2.1. Materials and instruments

The monomer 3-((2,2′:5′,2″-terthiophen)-3′-yl)-5-aminobenzoic acid the (TTABA) and N, S-doped porous carbon was freshly synthesized. For the synthesis of TTABA, 3′-Bromo-2,2′:5′,2″-terthiophene (BTT) was initially synthesized using 2-bromothiophene and 2,3,5-tribromothiophene. L-Lactate dehydrogenase (LDH) (EC) number 1.1.1.27 from rabbit muscle, sodium L-lactate (98%), NAD^+ (disodium hydrate), bovine serum albumin (BSA), β-nicotinamide adenine dinucleotide (NADH) were purchased from Sigma-Aldrich (USA). The detail of the required materials and instruments used in the experiments can be found in the Supplementary information under Section 1.1.

2.2. Synthesis of N, S-doped porous carbon (DPC)

The DPC was produced by previously reported method (Naveen et al., 2017a, b). Briefly, Zn-dithiooxamide (Zn-DTO) framework was synthesized and carbonized at appropriate temperature under a nitrogen atmosphere. Black colored N, S-doped porous carbon was obtained and washed with an excess amount of distilled water and ethanol followed by completely dry in a vacuum drier for further experiments. Detail synthesis of DPC can be found in the Supplementary information under Section 1.2.

2.3. Fabrication of the sensing probe

Prior to the modification of sensing layer, the glassy carbon (GC) electrode was polished to a mirror finish with alumina slurry 0.3 and 0.05 μM. Freshly prepared DPC 1 mg was suspended into 1 mL of H_2O and sonicated for 30 mint to obtain a homogenous suspension and drop-casted onto GC surface. Then, bi-functionalized CP was electrochemically polymerized by the potential cycling between 0.0 and +1.3 V for three cycles in an acetonitrile solution containing a monomer (TTABA) and 0.1 M tetrabutyl ammonium perchlorate (TBAP) as shown in (Fig. S1). After polymerization, the carboxylic acid group of the pTTABA was activated with 10.0 mM EDC/NHS for 6 h, followed by the subsequent incubation in 0.1 M PBS containing 1 mg/1 mL solution of NAD^+ at 4 °C for 6 h. The electrode was then immersed in a BSA solution to block unreacted sites. Through this step, NAD^+ was immobilized by the covalent bond formation with carboxylic acid groups of CP. After that, the NAD^+-pTTABA/DPC electrode was immersed into 0.1% glutaraldehyde diluted in PBS containing 1 mg/1 mL solution of LDH at 4 °C, followed by the reaction for blocking the unreacted sites and washing steps. Finally, the modified electrode (LDH/NAD^+)-pTTABA/DPC was used for lactate detection. Additionally, a control sensor probe (CSP) was fabricated by immobilizing NAD^+ and LDH onto the –COOH terminal of pTTABA and leaving the $–NH_2$ group in the unreacted state. To do this, the similar procedure was applied as mentioned above for DPC and pTTABA layer formation and activation by the EDC/NHS. Through this step, NAD^+ and LDH were immobilized at –COOH functional group terminal of pTTABA and the CSP was tested for lactate sensing. In the immobilization process, the EDC/NHS coupling reaction has been most feasible in pH 4.5, however, to maintain a complete physiological condition on the electrode surface for NAD^+ and LDH, the reaction was

carried at pH 7.

2.4. Preparation of mammalian cells and drug treatment

Normal cells (Vero) and cancer cells (MCF-7 and HeLa) were cultured separately in a DME medium containing 10% heat inactivated fetal bovine serum, 100 units/mL of penicillin and 100 units/mL of streptomycin in a T75 culture flask at constant 37 °C under 5% CO_2 and 95% humidity in a CO_2 incubator. The culture media were replaced once after two days until 95% confidence was obtained and then sub cultured. To detect extracellular lactate, the media from each cell culture containing the extra cellular releases were collected carefully without disturbing the cells and assayed for lactate determination. Cells were treated with αCHC according to the following procedure. The drug was diluted from stock solutions and applied onto the cells at 1:100–1:500 concentrations; cultured cells with and without αCHC were incubated at 37 °C thereafter, the effect of αCHC was evaluated in term of extracellular lactate detection.

2.5. Electrochemical detection of lactate

The analytical performance of the modified (LDH/NAD^+)-pTTABA/DPC probe was investigated using various electrochemical methods. Cyclic voltammograms (CVs) were recorded from 0.0 to +0.6 V versus Ag/AgCl in a 0.1 M PBS (pH 7.5). Under optimized conditions, the chronoamperograms were recorded at the applied potential of +0.35 V using the successive addition of lactate into the electrochemical cell containing 0.1 M PBS (pH 7.5).

3. Results and discussion

The detection mechanism of lactate is based on the oxidation of lactate to pyruvate by LDH in the presence of nicotine amide adenine dinucleotide (NAD^+). The enzymatic reactions involved in the biosensing system are as follows:

LDH

$$\text{Lactate} + NAD^+ \rightarrow \text{Pyruvate} + \text{NADH} + H^+ \quad (1)$$

$$\text{NADH} \rightarrow NAD^+ + H^+ + 2e^- \quad (2)$$

Reaction (1) is lactate dependent, whereas the oxidation of NADH at the electrode surface reaction (2) is directly proportional to the lactate concentration in the solution. Thus, we fabricated the proposed sensor as summarized in Scheme 1, showing that NAD^+ and LDH were separately immobilized onto carboxylic and amine terminals of bi-functionalized CP formed at N, S-doped porous carbon layer. Each layer of the sensor probe was characterized using FE-SEM, XPS, EIS, and CV, and the sensor was evaluated by detecting lactate in biological matrices.

3.1. Surface characterization of the sensor probe

The surface morphology of each sensor layer was investigated by FE-SEM as shown in (Fig. S2). The images were obtained for (a) as prepared DPC, (b) after pTTABA polymerization on DPC, (c) attachment of NAD^+ onto pTTABA/DPC layer, and (d) immobilization of LDH onto NAD^+-pTTABA/DPC layer. The DPC was in a regular spherical shape and the size was around 900 ± 100 nm as shown in (Fig. S2 (a)). The morphology after pTTABA polymerization revealed a smooth layer covering on the DPC as shown in (Fig. S2 (b)). The attachment of NAD^+ on the pTTABA/DPC layer appeared as small particles as depicted in (Fig. S2 (c)), this could be due to the covalent bond formation between NAD^+ and the CP. Similarly, the surface showed rough morphology after the immobilization of LDH as shown in (Fig. S2 (d)).

In addition, the XPS analysis was performed to confirm the sensing electrode modification. All XPS spectra were taken after 20 s of Ar ion gas etching and calibrated using the C1s peak at 284.6 eV as an internal standard as shown in (Fig. 1 (A)). XPS data were obtained for (I) as prepared DPC, (II) after pTTABA polymerization on DPC, (III) attachment of NAD^+ onto pTTABA/DPC layer, and (IV) immobilization of LDH onto NAD^+-pTTABA/DPC layer. The survey spectra in (Fig. 1 A (a)) show O1s, C1s, and N1s, and S2p peaks for all the surfaces at 531.9, 284.2, 399.9, and 163.3 eV, respectively. The P2p peak is present in the layer (III) at 133.2 eV, whereas the peak is not appeared for layer (II), which indicates that NAD^+ is successfully immobilized on the CP surface. Further, the intensity of N1s peak is gradually increased from layer (I) to (IV), which is owe to an increase in nitrogen content after stepwise attachment of the sensor materials having N atom. The deconvoluted C1s spectrum of pTTABA/DPC exhibits two peaks at 284.6 and 286.4 eV,

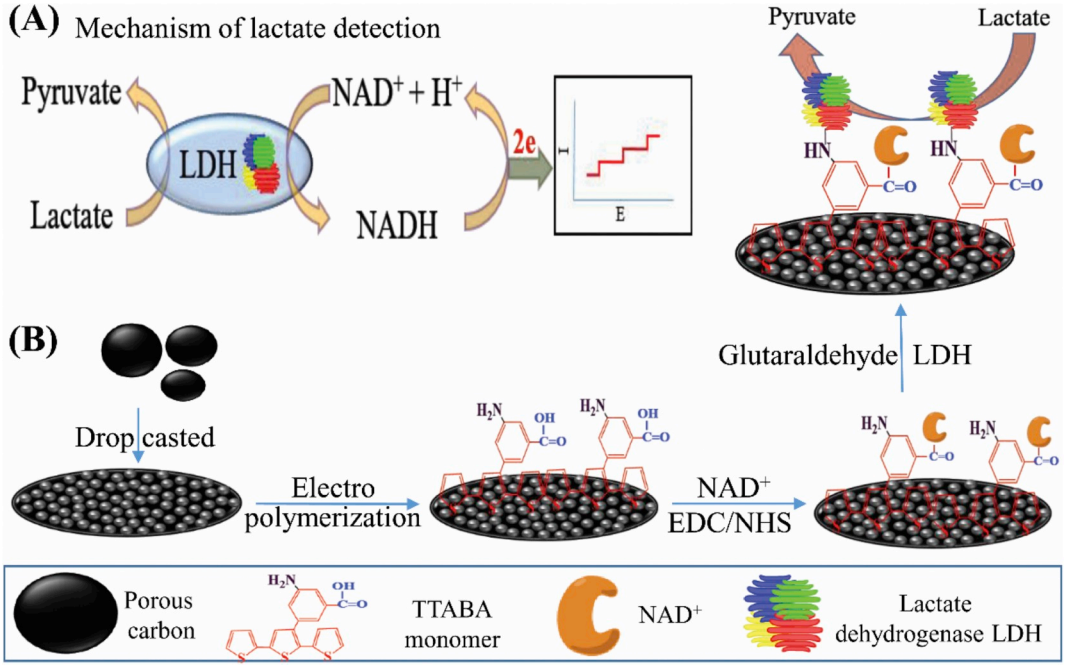

Scheme 1. Schematic representation for the fabrication of lactate sensor.

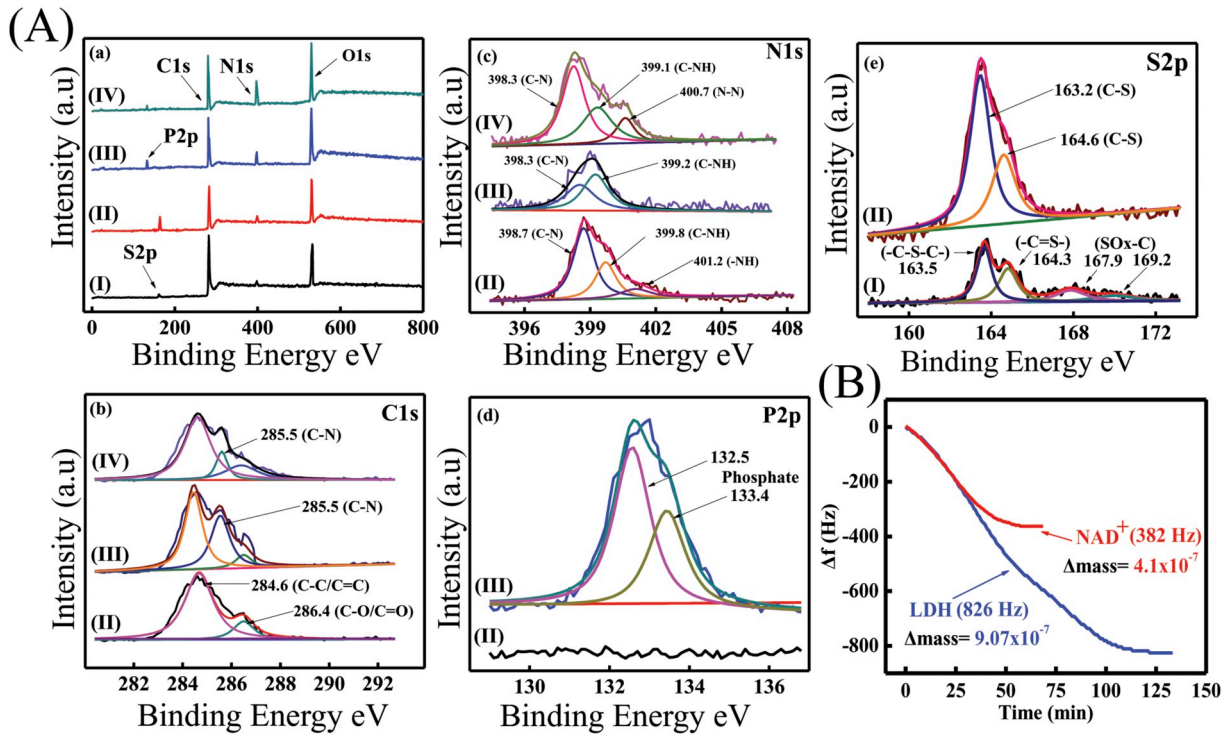

Fig. 1. (A) XPS analysis of (a) survey spectra obtained for (I) as prepared N, S-doped porous carbon (DPC), (II) pTTABA/DPC, (III) NAD^+-pTTABA/DPC, and (IV) (LDH/NAD^+)-pTTABA/DPC. (b) and (c) deconvoluted C1s and N1s spectra obtained for layer (II), (III), and (IV) respectively. (d) deconvoluted P2p spectra obtained for layer (II) and (III) and (e) S2p spectra obtained for layer (I) and (II). (B) Frequency changes during the immobilization of NAD^+ and LDH onto the modified electrode surface.

which correspond to the C–C, C–H, and/or C–S, and C= O, C–O bonds, as shown in (Fig. 1A b (II)). However, an additional peak is observed at 285.5 eV after the amide bond formation between amine groups of NAD^+ and carboxylic groups of pTTABA as shown in (Fig. 1A b (III– IV)). In addition, the deconvoluted N1s spectrum was obtained for layer (II), (III), and (IV) as shown in (Fig. 1 A (c)). Layer (II) shows three peaks at 398.7, 399.8, and 401.1 eV, which correspond to C–N, C═NH, and –NH respectively. Further, two peaks were observed for the layer (III) that shifted to lower binding energy from 398.7 to 398.3 and 399.8 to 399.2 eV corresponding to C–N and –NH bond, respectively. The small shift in binding energy is owe to the formation of amide bond between the carboxylic groups of CP and amine groups of NAD^+. However, an additional peak at the layer (IV) is observed at 400.7eV, which is absent in the layer (III) corresponding to the N–N bond formation (Verma et al., 2013) between the amine groups of LDH and CP. The deconvoluted P2p spectrum in (Fig. 1 A (d)) shows two distinctive peaks for the layer (III) at 132.67 and 133.67 eV corresponding to the phosphate atoms in the NAD^+ molecule. However, these peaks are absent in the layer (II). The deconvoluted S2p spectrum in (Fig. 1 A (e)) shows two peaks for the layer (II) at 163.2 and 164.6 eV, corresponding to C–S for the polymer modified surface and the S2p electron of sulfur present in the TTABA monomer (Hussain et al., 2016). Otherwise, in case of DPC layer (I), four distinctive peaks are observed at 163.5, 164.3, 167.9, and 169.2 eV corresponding to –C-S-C, –C═S-, and SOx-C respectively (Naveen et al., 2017a, b). These results confirm the successful polymerization of pTTABA onto the DPC layer as well as immobilization of NAD^+ and LDH onto the pTTABA/DPC composite.

3.2. Quantification of immobilized NAD^+ and LDH

QCM experiments were performed to quantify the amount of NAD^+ and LDH attached onto the sensing electrode surface. During the immobilization of NAD^+ and LDH, the frequency decreased and attained a steady state after 75 and 135 min for NAD^+ and LDH respectively, as shown in (Fig. 1 (B)). The frequency change (Δf) was calculated to be ($\Delta f = 382$ and 826 Hz) for NAD^+ and LDH as shown in (Fig. 1 B curve (a-b)), respectively, and it was converted to mass change using the equation reported previously (Chung et al., 2018), and the amount of NAD^+ and LDH immobilized on the pTTABA/DPC modified electrode was 4.1 $\times 10^{-7}$ and 9.07 $\times 10^{-7}$ g, with surface coverage of 3.12 $\times 10^{-9}$ and 3.3 $\times 10^{-11}$ mol/cm^2 for NAD^+ and LDH, respectively. The obtained results sufficiently confirm the successful immobilization of NAD^+ and LDH onto carboxylic and amine terminal of pTTABA, respectively. These results are in a good agreement with the XPS analysis.

3.3. Electrochemical properties of the sensor probe

To examine the surface electrical characteristic of the sensor probe, EIS was performed in the presence of $(Fe(CN)_6)^{3-/4-}$ and the frequency was scanned from 100 kHz to 100 mHz at an open circuit voltage. The EIS spectra (Fig. 2 (A)) were obtained for (a) as prepared DPC, (b) pTTABA/DPC, (c) NAD^+-pTTABA/DPC and (d) (LDH/NAD^+)-pTTABA/DPC. Each parameter was determined by fitting the experimental results to a Randle circuit using a Zview 2 impedance software. The circuit is shown in the inset of (Fig. 2 (A)), where Rs is the solution resistance, Rp1 and Rp2 are the polarization resistances, W represents the Warburg impedance (ZW), and Q_{dl} & Q_f denote the constant phase elements (CPE), representing double-layer capacitance and film capacitance, respectively. After fitting the experiment data, the R_{ct} values were found to be 0.5, 1.2, 2.7, and 3.4 KΩ for layer (a) to (d) respectively. The gradual increase in the interfacial impedance between the modified layers clearly validates the successful fabrication of each sensing layer.

In addition, a series of control experiments using CV was carried out to validate the sensing layer. At first, CVs were recorded between −0.05 V and +0.600 V in a 0.1 M PBS containing 1 mM of lactate for (a) as-prepared DPC, (b) pTTABA/DPC, (c) NAD^+-pTTABA/DPC, (d) (LDH/NAD^+)-pTTABA and (e) (LDH/NAD^+)-pTTABA/DPC as shown in Fig. 2 (B). As expected, no CV peak was observed in the layers (a), (b), and (c),

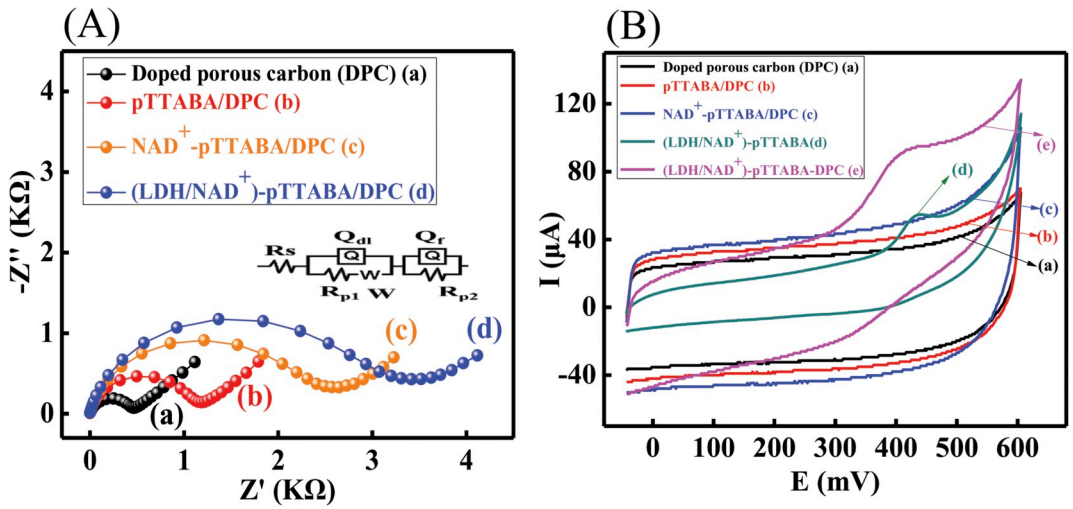

Fig. 2. (A) EIS spectra obtained for (a) as prepared DPC, (b) pTTABA/DPC, (c) NAD^+-pTTABA/DPC and (d) (LDH/NAD^+)-pTTABA/DPC in $(Fe(CN)_6)^{3-/4-}$ solution. (B) CVs recorded for (a) as prepared DPC, (b) pTTABA/DPC, (c) NAD^+-pTTABA/DPC, (d) (LDH/NAD^+)-pTTABA and (e) (LDH/NAD^+)-pTTABA/DPC in 0.1 M PBS containing 1.0 mM lactate.

this is owed to the absence of the catalytic enzyme (LDH) on the electrode surface. However, a clear oxidation peak was observed at + 0.430 and + 0.400 mV in CVs recorded for (d) and (e) respectively, corresponding to the oxidation of NADH that generated by the catalytic effect of LDH. It is worth to note that the peak current was increased by 39.2 μA and the negative shift in the potential was observed in CV (e) when N, S doped porous carbon was coated onto the electrode surface as compared (d) without DPC coated electrode. It clearly indicates that N, S doped porous carbon is an excellent catalytic material for NADH oxidation. The presence of NADH oxidation peak is directly related to

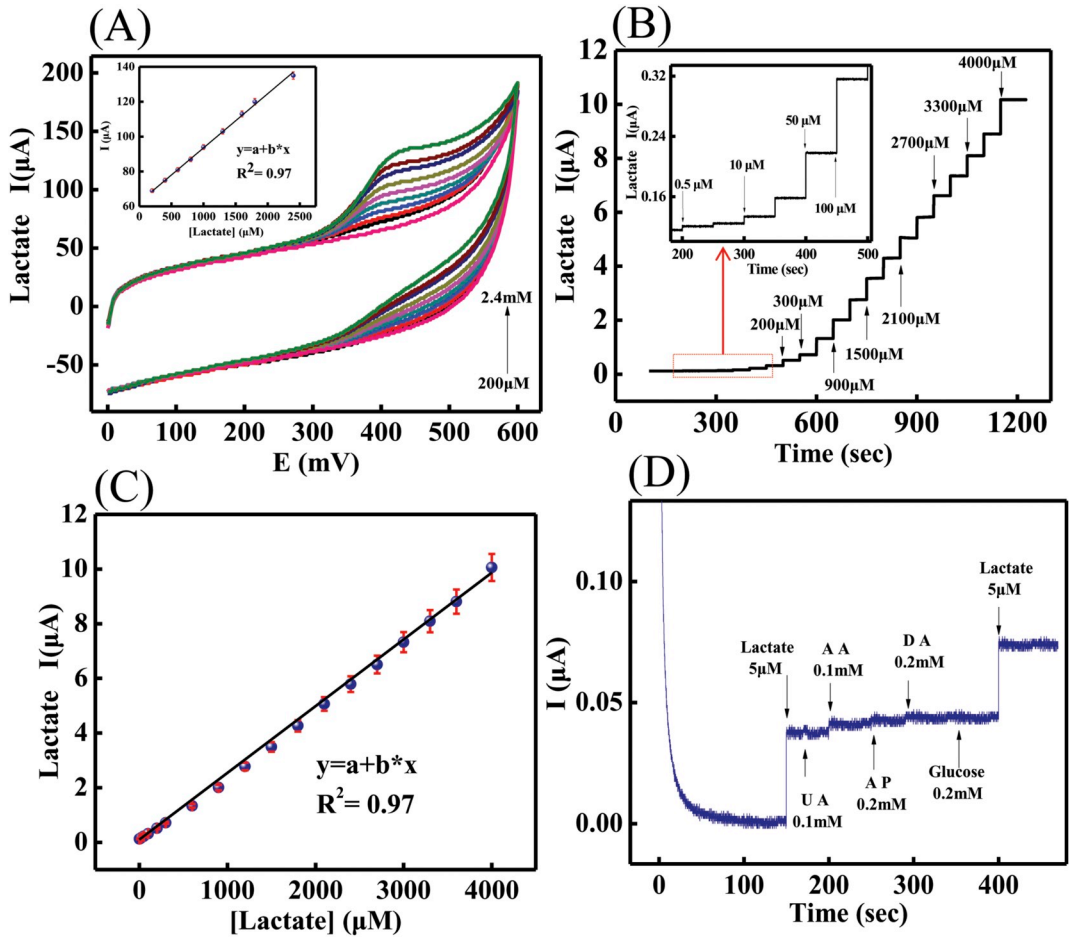

Fig. 3. (A) CVs recorded for various concentration of lactate ranging from 200.0 μM to 2.4 mM in a 0.1 M PBS, the inset showing the calibration plot of the same. (B) Chronoamperometric responses toward various lactate concentrations in a 0.1 M PBS. (C) Calibration plot and (D) the response of the potential interfering agent.

lactate as explained earlier in equations (1) and (2). The porous carbon material without the doping of nitrogen and sulfur was previously tested for its catalytic activity and found that the activity dramatically increased with doping of duel hetero atoms (Naveen et al., 2017a, b). Furthermore, to evaluate the analytical performance of the DPC with other mere carbon materials, various sensors were fabricated using multiwalled carbon nanotube (MWCNT), graphene, reduced graphene oxide (rGO) and tested for lactate detection as shown in (Fig. S3). When DPC was used, the results clearly showed that the signal increased by 65 μA, 56 μA, 48 μA as compared to that of MWCNT, graphene, and rGO, respectively. Beside the enhancement in the current, a negative shift in the potential was observed for DPC about 90, 80, and 50 mV for MWCNT, graphene, and rGO, respectively. The obtained results adequately confirm the excellent catalytic activity of DPC compared with other mere carbon materials, which could be due to the presence of N, S atoms and their carbon bonds in the porous carbon.

To investigate the sensing performance of the proposed sensor towards lactate, a series of CVs were recorded between 0.0 and +0.60 V in a 0.1 M PBS containing various concentrations of lactate ranging 200, 400, 600, 800 μM and 1.0, 1.4, 1.6, 1.8, 2.2, and 2.4 mM as shown in (Fig. 3 (A)). The corresponding calibration plot in the inset of (Fig. 3 (A)) displays good linearity between various lactate concentrations and the obtained current responses. To confirm the signal shown in (Fig. 3 (A)) that was due to the oxidation of NADH, a control experiment was performed using the standard NADH solution (Fig. S4). A series of CVs were recorded between 0.0 and +0.60 V in a 0.1 M PBS containing various concentrations of NADH ranging 50 μM to 3.5 mM. The CVs reveal that upon increasing NADH concentration, the peak current was increased linearly. The calibration plot was obtained with the R^2 value of 0.98 as shown in the inset of (Fig. S4).

3.4. Optimization of the detection parameters

Various experimental parameters were optimized, such as temperature, pH, applied potential, and TTABA monomer concentration as shown in (Fig. S5). The effect of temperature on the proposed sensor was studied from 20 to 45 °C (Fig. S5 (a)). The response current of lactate was increased gradually and reached the maximum at 35 °C, and thereafter it was decreased, which could be due to the denaturation of the biomolecules present at the modified electrode surface, hence 35 °C was selected as an optimum temperature. A similar trend was observed in case of optimization (Fig. S5 (b)), where the highest current was observed at pH 7.5, hence it was selected as an optimal pH for further experiments. The effect of applied potential was studied from +250 + 450 mV (Fig. S5 (c)), a gradual increase in response was observed from +250 to +300 reaching maximum at +350 mV and thereafter it decreased; hence +350 mV was selected for chronoamperometric experiments. The monomer concentration was investigated in the range of 0.5–2.5 mM (Fig. S5 (d)), the results showed a gradual increase in response, where it reached maximum at 1.5 mM. However, after 1.5 mM, a decrease in signal was observed, hence, 1.5 mM was chosen as an optimum concentration, and the decrease in response after 1.5 mM could be due to the increase in the thickness of the polymerized layer formed on the electrode surface. All optimized parameters were selected for further experiments.

3.5. Performance comparison between bi and single terminal CPs

To investigate the performance of the proposed sensor and the control sensor fabricated by single terminal CP (pTTABA) immobilization, chronoamperometric experiments were carried out under optimized conditions. At first, the analytical performance of the proposed sensor probe using pTTABA was evaluated by detecting lactate in varied concentrations in 0.1 M PBS (Fig. 3 (B)). A typical chronoamperogram was obtained by the successive addition of lactate in the measuring solution. The corresponding calibration plot (Fig. 3 (C)) exhibited a good linearity with a dynamic range from 0.5 μM to 4.0 mM. The lactate analysis yielded a linear equation of Ip (μA) = 1.12 (±0.031) + 0.02 (±0.00031) (Lactate) (μM/mL) with a correlation coefficient of 0.97. The sensitivity of the sensor (the slope of this plot) is 0.02 ±μA mL/μM. The detection limit of lactate is determined to be 0.112 ± 0.02 μM, based on five measurements for the standard deviation of the blank noise (95% confidence level, signal noise ratio k = 3). The analytical performance of the proposed method compared to previous reports are summarized in Table S1, where the proposed method clearly shows a superior performance in terms of the detection limit and dynamic range. On the other hand, the performance was similarly evaluated for the control sensor using CSP for the detection of lactate in varied concentrations in 0.1 M PBS as shown in (Fig. S6). The results showed a linear relationship between current and the increment in lactate concentration, where the linear range was obtained from 5 to 300 μM. The linear dependencies of lactate analysis yielded an equation of Ip (μA) = 0.0084 (±0.02) + 0.01 (±0.00021) (Lactate) (μM/mL) with a correlation coefficient of 0.91 as shown in inset (Fig. S6). The sensitivity of the sensor (the slope of this plot) was 0.01 ± μA mL/uM. The detection limit of lactate is determined to be 0.95 ± 0.04 μM, based on five measurements for the standard deviation of the blank noise (94% confidence level, signal noise ratio k = 3). These results show that when NAD^+ and LDH were immobilized onto two separate ends of pTTABA, the analytical performance of the proposed sensor probe was superior in terms of sensitivity, detection limit, and linear range compared when NAD^+ and LDH were immobilized onto single end (-COOH) of pTTABA. This could be due to the higher amount of cofactor and enzyme immobilized stably onto the electrode surface.

3.6. Interference study, reproducibility, and stability

To evaluate the selectivity of the proposed sensor, chronoamperometry was performed in the presence of common biological interfering species, such as 0.1 mM uric acid (UA), 0.1 mM ascorbic acid (AA), 0.2 mM acetaminophen (AP), 0.2 mM dopamine (DA), and 0.2 mM glucose. The interfering agents were added turn wise into the measuring solution containing 0.1M PBS as shown in (Fig. 3 (D)). The obtained results showed insignificant current responses upon their addition into the measuring solution. However, when lactate (5 μM) was introduced into the same solution a clear peak was observed. The result confirms that the sensor probe exhibited sufficient selectivity for the determination of lactate, which is due to the highly specific enzyme reactions. Further, the relative standard deviation (RSD) was calculated and found to be 3.17% when five different electrodes were used to detect lactate in three different concentrations (300, 2200, and 4000 μM) as shown in (Fig. S7), the obtained result showed good electrode-to-electrode reproducibility. Finally, to investigate the stability of the sensor, it was stored at 4 °C for 60 days as shown in (Fig. S8). The amperometric measurements were carried out at regular interval (5 days), which shows insignificant change in response, indicated that the sensor probe is highly stable, which could be due to the stable immobilization of NAD+ and LDH on the pTTABA layer.

3.7. Real sample analysis and the effect of αCHC on lactate efflux at cancer cells

The applicability of the sensor probe was investigated by detecting lactate in the extracellular matrix of Vero, MCF-7, and HeLa cells. At first, the aliquots of the bathing medium (3 mL) from each cell line were collected carefully and transferred to the electrochemical cell for its assay using chronoamperometry. In the first set of experiment, aliquots were collected from various numbers of Vero, MCF-7, and HeLa ranging from 2, 4, 6, 8 and 10 × 10^6 cells and assayed to determine the lactate variation among them as shown in (Fig. 4 (A)). The results depicted that as the cell number increased, the response current of lactate was also enhanced for all cells. Further, the current enhancement in normal cell

(Vero) was minimal, when the cell number was increased, however, the current response of lactate was 2.4 and 6.4 μA higher for MCF-7 and HeLa, respectively as compared to that of Vero response. Among the cancer cells, the response of HeLa was 2.4 μA higher than that of MCF-7. The difference in the extracellular lactate concentration between normal and cancer cells could be due to the altered metabolic pathway in cancer cells (Warburg effect), the high glycolysis rate in cancer cells produces lactic acid from glucose fermentation, hence the level of lactic acid is more in the extracellular space in cancer cells (Cairns et al., 2011). Further, the difference in lactate response current between cancer cells is due to the presence of MCTs type and cancer cell origin. For instance, HeLa cells express both types of lactate transporter (MCT 1 and MCT4) (Ullah et al., 2006; Gallagher et al., 2007), therefore the level of extracellular lactate is more in HeLa compared to that of MCF-7, which mainly express MCT1 (Slomiany et al., 2009). Further, the origin of both cancer cells is different, hence they differ in MCT expression (Pérez et al., 2016). Additionally, chronoamperometric responses were recorded with and without αCHC treatment using an equal number of Vero, MCF-7, and HeLa cells (6×10^6) as shown in the inset of (Fig. 4 (B)). The obtained results in (Fig. 4 (B)) showed a similar trend, where the level of lactate decreased for all cell lines after αCHC treatment. The lactate signal decreased by 28, 90, and 42% for Vero, MCF-7, and HeLa cells, respectively compared with the response without treatment. The lower blocking effect of the drug in Vero cells could be due to the fact that Vero cells follow the normal metabolic pathway, hence the extracellular level of lactate is less. However, the prominent effect of the drug was observed in MCF-7 cells, which could be due to the expression of only (MCT1), hence the drug blocks the out flux of lactate in the extracellular matrix (Slomiany et al., 2009). In case of HeLa cells, the effect was somewhat significant because HeLa express both MCT1 and MCT4. Furthermore, the affinity of αCHC for MCT4 is approximately 5 times lower; thus, the inhibitory effect of the drug on MCT4 is less compared to MCT1, which leads to higher levels of extracellular lactate in HeLa cells than that of MCF-7 cells after αCHC treatment (Sharpe et al., 2003).

To study the cytotoxic role of αCHC in term of its time dependency and concentration profile, chronoamperometery was performed to detect the extracellular lactate in Vero, MCF-7, and HeLa using an equal number of cells in all experiments (6×10^6) at a fixed concentration of 200 μM of αCHC. The time dependency profile was obtained after 0, 12, 24, 36, and 48 h treatment with αCHC as shown in (Fig. 5 (A)). The results showed that as the treatment time increased, the current response of lactate in the extracellular space of both cancer cells was decreased and reached minimum at 36 h, thereafter no further decrease in current was observed for cancer cell lines. However, normal cells were unaffected by the treatment of αCHC hence no significant change in current was observed during the treatment time. The decrease in the current response for MCF-7 and HeLa cells can be attributed to the accumulation of lactate inside the cells due to the blocking effect of αCHC onto lactate efflux. The details of the cell viability in % is shown in Table S2. Similarly, the concentration dependency profile was established as shown in (Fig. 5 (B)). The experiment was carried out using various drug concentrations ranging from (0, 50, 100, 150, 200, 250, and 300) μM of αCHC. The results showed that the maximum inhibitory effect was observed when 200 μM was used for both cancer cells, where the cytotoxic effect was more prominent in the case of MCF-7, however, no significant change in current response was observed in case of normal cells. The cell viability using different concentrations of αCHC after 36 h treatment is summarized in Table S3. Further, to confirm these results, optical microscopic images were taken at 36 h and 200 μM αCHC as shown in (Fig. S9 (A-B)), respectively, for (I) control sample without αCHC, with the treatment of αCHC for (II) Vero, (III) MCF-7, and (IV) HeLa. Before taking the images, general procedure was applied to differentiate viable and non-viable cells using trypan blue staining. Nonviable cells are in blue color and viable cells remain unstained. The images depicted that MCF-7 cell were most affected by the administration of αCHC followed by HeLa and Vero, this could be due to the reasons given above regarding to the specificity of the drug and the type of MCT expression. Similarly, the optical microscopic images were taken after 36 h for (I) control sample without αCHC, and with αCHC at 200 μM for (II) Vero, (III) MCF-7, and (IV) HeLa cells. As expected, similar results were obtained to that of time dependency profile in term of the high toxic effect of the drug to MCF-7 compared to HeLa cells with minor effect onto the Vero cells. Overall, the effect of αCHC on normal cells was minimal, however; the effect was prominent in case of cancer cells, where the blocking effect of the drug was higher for MCF-7 compared to HeLa cells.

4. Conclusions

A highly sensitive and selective amperometric nano biosensor was successfully developed using separately bonded NAD^+ and LDH on a bi-functionalized conducting polymer composited with N, S-doped porous carbon for the extracellular lactate detection in cancer cells. Enhanced sensitivity, selectivity, stability, lower detection limit and broader dynamic range were observed for the proposed sensor due to separately bound biocatalysts and the higher catalytic activity of the electrode surface materials. The proposed sensor was successfully applied for the detection of lactate in the extracellular matrix of non-cancerous (Vero)

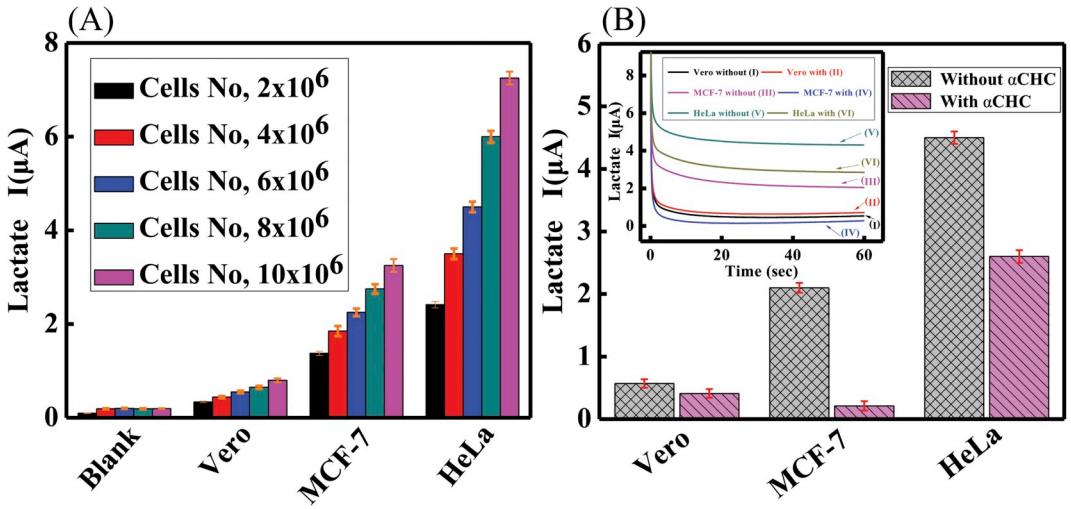

Fig. 4. Lactate response for various numbers of cells for Vero, MCF-7, and HeLa ranging from 2, 4, 6, 8, and 10×10^6 cells. (B) Lactate response recorded with and without αCHC employing the same cell lines, and the inset shows the amperometric response.

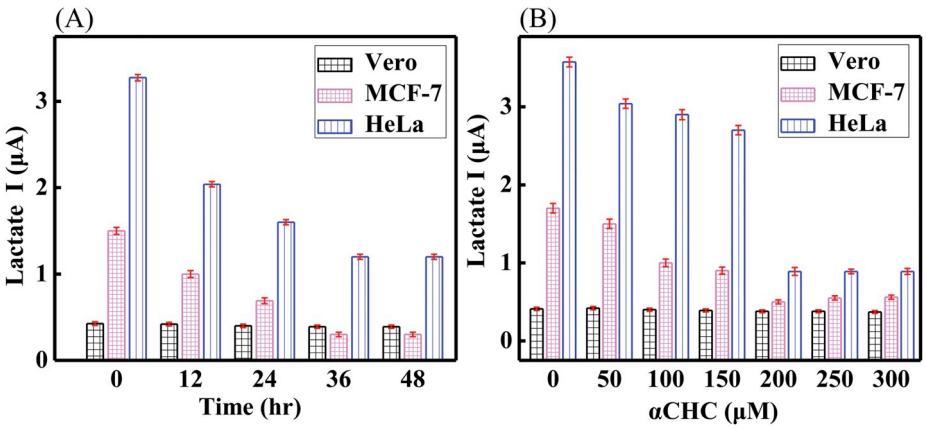

Fig. 5. (A) Time dependency profile of 200 μM of αCHC obtained at (0, 12, 24, 36, and 48 h). (B) Concentration profile at 36 h employing various concentrations of αCHC (0, 50, 100, 150, 200, 250, and 300 μM).

and two cancerous cell lines (MCF-7 and HeLa). This confirmed the higher concentration of lactate in the extracellular release of HeLa than MCF-7 and Vero. Furthermore, the sensor was employed to compare the blocking effect of αCHC inhibitor onto MCT using the same cell lines, where the lactate concentrations after αCHC treatment were decreased by 28, 90, and 42% in Vero, MCF-7, and HeLa cells, respectively. Finally, the time and concentration dependency profile of αCHC on the cell viability was perceived, and the highest toxic effect was observed after 36 h of treatment at 200 μM. The proposed sensor probe adequately confirmed the cytotoxic effect of αCHC on the breast cancer cell lines, hence it could be applied as a drug/supplement in the treatment of breast cancer rather than another types of cancers. This method has the potential in diverse clinical and pharmaceutical applications and can be extended into the screening and development of other potential anti-tumor drugs.

Declaration of competing interest

The authors declare that they have no known competing financial interests or personal relationships that could have appeared to influence the work reported in this paper.

Acknowledgments

This work was supported by the National Research Foundation of Korea (NRF), grant funded by the Korea government (MSIP) (No. 2019R1A2C1002531).

Appendix A. Supplementary data

Supplementary data to this article can be found online at https://doi.org/10.1016/j.bios.2020.112094.

References

Akhtar, M.H., Mir, T.A., Gurudatt, N.G., Chung, S., Shim, Y.B., 2016. Biosens. Bioelectron. 85, 488–495.
Braendlein, M., Pappa, A.M., Ferro, M., Lopresti, A., Acquaviva, C., Mamessier, E., Malliaras, G.G., Owens, R.M., 2017. Adv. Mater. 29 (13), 1605744.
Cairns, R.A., Harris, I.S., Mak, T.W., 2011. Nat. Rev. Canc. 11 (2), 85–95.
Chung, S., Chandra, P., Koo, J.P., Shim, Y.B., 2018. Biosens. Bioelectron. 100, 396–403.
Colen, C.B., Shen, Y., Ghoddoussi, F., Yu, P., Francis, T.B., 2011. Neoplasia, vol. 13, pp. 620–632.
Estrella, V., Chen, T., Lloyd, M., Wojtkowiak, J., Cornnell, H.H., Ibrahim-Hashim, A., Bailey, K., Balagurunathan, Y., Rothberg, J.M., Sloane, B.F., Johnson, J., 2013. Canc. Res. 73 (5), 1524–1535.
Gallagher, S.M., Castorino, J.J., Wang, D., Philp, N.J., 2007. Canc. Res. 67 (9), 4182–4189.
Galluzzi, L., Kepp, O., Vander Heiden, M.G., Kroemer, G., 2013. Nat. Rev. Drug Discov. 12 (11), 829–846.
Hamdan, L., Arrar, Z., Al Muataz, Y., Suleiman, L., Negrier, C., Mulengi, J.K., Boukerche, H., 2013. PloS One 8 (9), e72953.
Hirschhaeuser, F., Sattler, U.G., Mueller-Klieser, W., 2011. Canc. Res. 71 (22), 6921–6925.
Hussain, K.K., Gurudatt, N.G., Mir, T.A., Shim, Y.B., 2016. Biosens. Bioelectron. 83, 312–318.
Kim, H.S., Masko, E.M., Poulton, S.L., Kennedy, K.M., Pizzo, S.V., 2012. BJU Int. 110, 1062–1069.
Kwon, N.H., Rahman, M.A., Won, M.S., Shim, Y.B., 2006. Anal. Chem. 78, 52–60.
Milagres, M.P., Brandão, S.C.C., Magalhães, M.A., Minim, V.P.R., Minim, L.A., 2012. Food Chem. 135 (3), 1078–1082.
Moon, J.M., Thapliyal, N., Hussain, K.K., Goyal, R.N., Shim, Y.B., 2018. Biosens. Bioelectron. 102, 540–552.
Naveen, M.H., Gurudatt, N.G., Shim, Yoon-Bo, 2017a. App. Mater. Today 9, 419–433.
Naveen, M.H., Shim, K., Hossain, M., Shahriar, A., Kim, J.H., Shim, Y.B., 2017b. Adv. Energy Mater 7, 1602002.
Nikolaus, N., Strehlitz, B., 2008. Microchimica Acta 160 (1–2), 15–55.
Park, D.S., Shim, Y.B., Park, S.M., 1993. J. Electrochem. Soc. 140 (10), 2749–2752.
Pérez-Escuredo, J., Van Hée, V.F., Sboarina, M., Falces, J., Payen, V.L., Pellerin, L., Sonveaux, P., 2016. Biochim. Biophys. Acta Mol. Cell Res. 1863 (10), 2481–2497.
Rathee, K., Dhull, V., Dhull, R., Singh, S., 2016. Biochemistry and Biophysics Reports 5, 35–54.
Romero-Garcia, S., Moreno-Altamirano, M.M.B., Prado-Garcia, H., Sánchez-García, F.J., 2016. Front. Immunol. 7, 52.
Sharpe, R.L., Milligan, C.L., 2003. J. Exp. Biol. 206 (3), 543–549.
Shim, Y.B., Won, M.S., Park, S.M., 1990. J. Electrochem. Soc. 137 (2), 538–544.
Slomiany, M.G., Grass, G.D., Robertson, A.D., Yang, X.Y., Maria, B.L., Beeson, C., Toole, B.P., 2009. Canc. Res. 69 (4), 1293–1301.
Sun, S., Wang, R., Huang, Y., Xu, J., Yao, K., Liu, W., Cao, Y., Qian, K., 2019. Small 15 (34), 1902441.
Ullah, M.S., Davies, A.J., Halestrap, A.P., 2006. J. Biol. Chem. 281 (14), 9030–9037.
Van Hall, G., 2010. Acta Physiol. 199 (4), 499–508.
Verma, M.L., Naebe, M., Barrow, C.J., Puri, M., 2013. PloS One 8 (9), e73642.
Whiteside, T.L., 2008. Oncogene 27 (45), 5904–5912.
Wu, F., Huang, Y., Huang, C., 2005. Biosens. Bioelectron. 21 (3), 518–522.
Zhang, R., Rejeeth, C., Xu, W., Zhu, C., Liu, X., Wan, J., Jiang, M., Qian, K., 2019. Anal. Chem. 91 (11), 7078–7085.